Electronic Supplementary Material to: Global Fire Emissions Linked to Madden–Julian Oscillation*

Young-Min YANG[1], Doo Young LEE[2], Jae-Heung PARK[3], June-Yi LEE[4,5], Kyung-Sook YUN[4,5], Soon-Il AN[6], Tim LI[7], and Bin WANG[7]

[1]*Department of Environment & Energy/School of Civil, Environmental Resources and Energy Engineering/Soil Environment Research Center, Jeonbuk National University, 567 Baekje-daero, Deokjin-gu, Jeonju-si, Jeonbuk State, South Korea*

[2]*Department Marine Sciences and Convergent Technology, Hanyang University, South Korea*

[3]*School of Earth and Environmental Sciences, Seoul National University, Seoul, South Korea*

[4]*Research Center for Climate Sciences, Pusan National University, Busan, South Korea*

[5]*Center for Climate Physics. Institute for Basic Science, Busan, South Korea*

[6]*Department of Atmospheric Sciences and Irreversible Climate Change Research Center, Yonsei University, Seoul, South Korea*

[7]*Department of Atmospheric Sciences and International Pacific Research Center, University of Hawaii, Honolulu HI, USA*

ESM to: Yang, Y.-M., D. Y. Lee, J.-H. Park, J.-Y. Lee, K. S. Yun, S.-I. An, T. Li, and B. Wang, 2025: Global fire emissions linked to Madden−Julian Oscillation. *Adv. Atmos. Sci.*, **42**(7), 1273−1284, https://doi.org/10.1007/s00376-025-4447-0.

*The online version of this article can be found at https://doi.org/10.1007/s00376-025-4447-0.

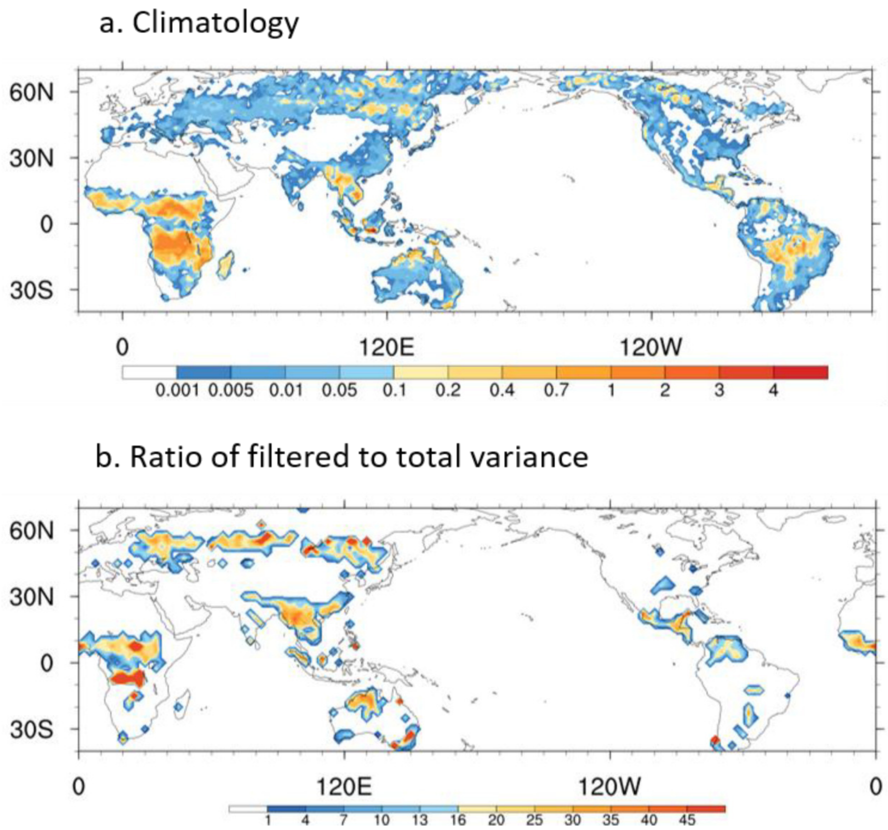

Fig. S1. Subseasonal variability of wildfire emissions. (a) Horizontal pattern of annual mean wildfire biomass burning carbon emissions (units: g C m^{-2} month^{-1}). (b) Ratio of the 20–70-day bandpass-filtered to total variance of wildfire emissions during February–April. Data for the years 2003–20 are used for the analysis.

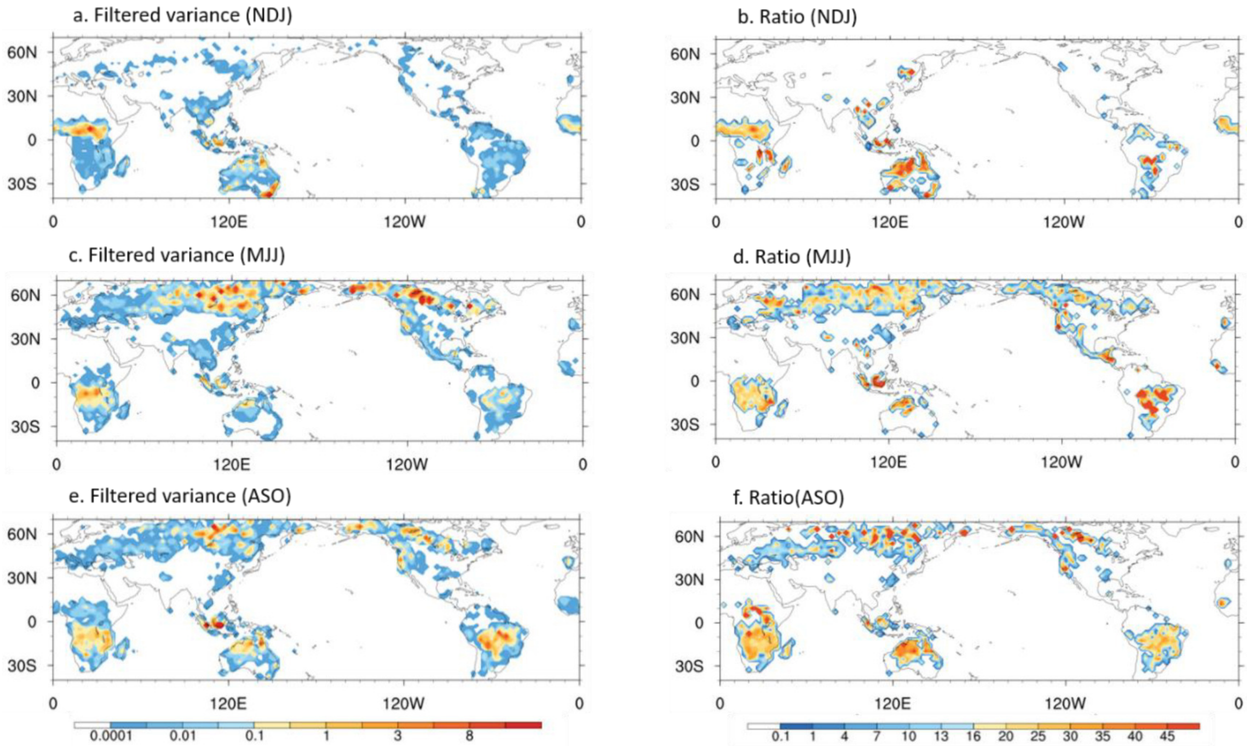

Fig. S2. Subseasonal variability of wildfire emissions. (a, c, e) 20–70-day bandpass-filtered wildfire emissions (units: g C m^{-2} $month^{-1}$) during (a) November–January, (c) May–June, and (e) August–October. (b, d, f) Ratio of the filtered to total variance of the wildfire emissions during (b) November–January, (d) May–June, and (f) August–October. Eighteen years (2003–20) of data are used for the analysis.

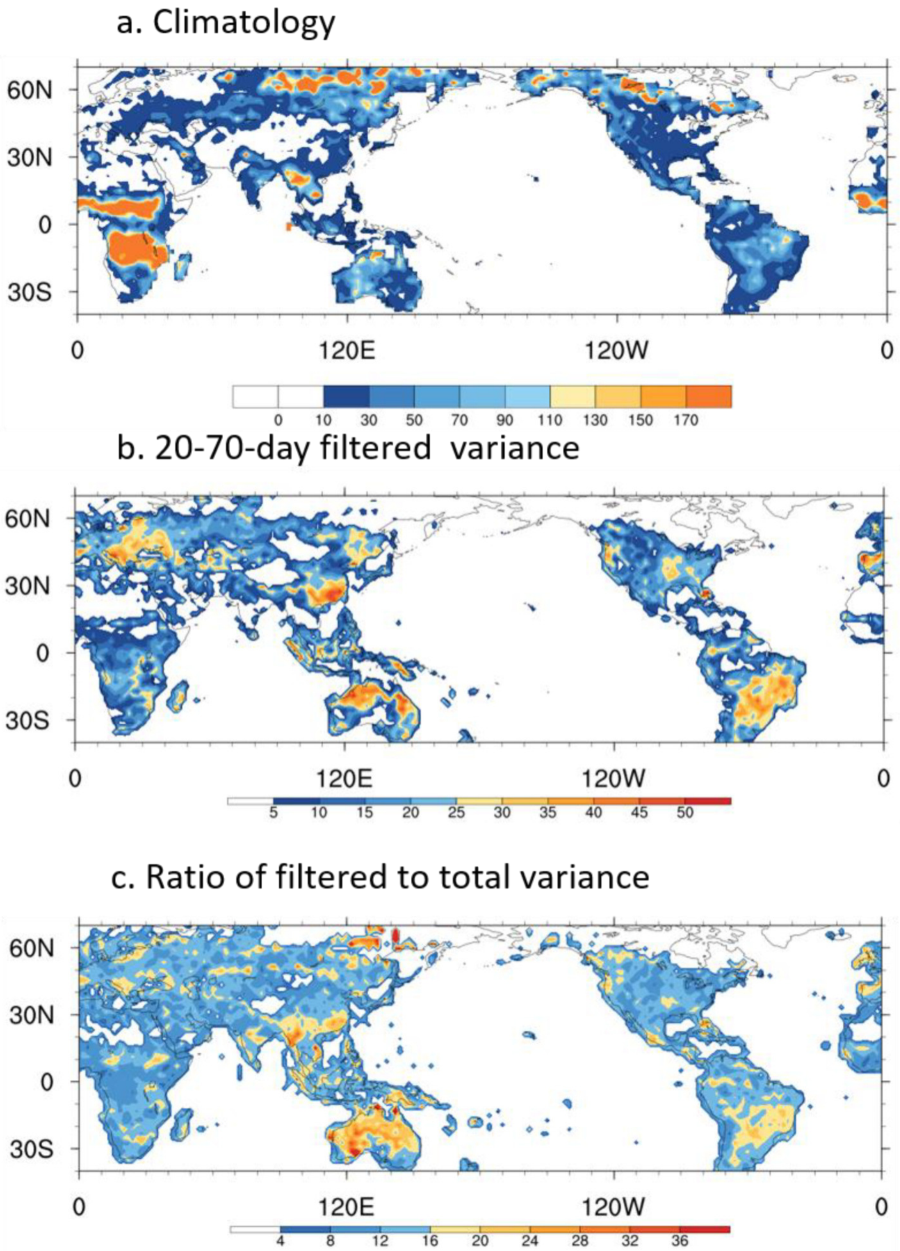

Fig. S3. Subseasonal variability of wildfire radiative power. (a) Horizontal pattern of annual mean wildfire radiative power (FRP; units: W m^{-2}). (b) 20–70-day bandpass-filtered FRP during February–April. (c) Ratio of the filtered to total variance of the FRP during February–April. Eighteen years (2003–20) of data are used for the analysis.

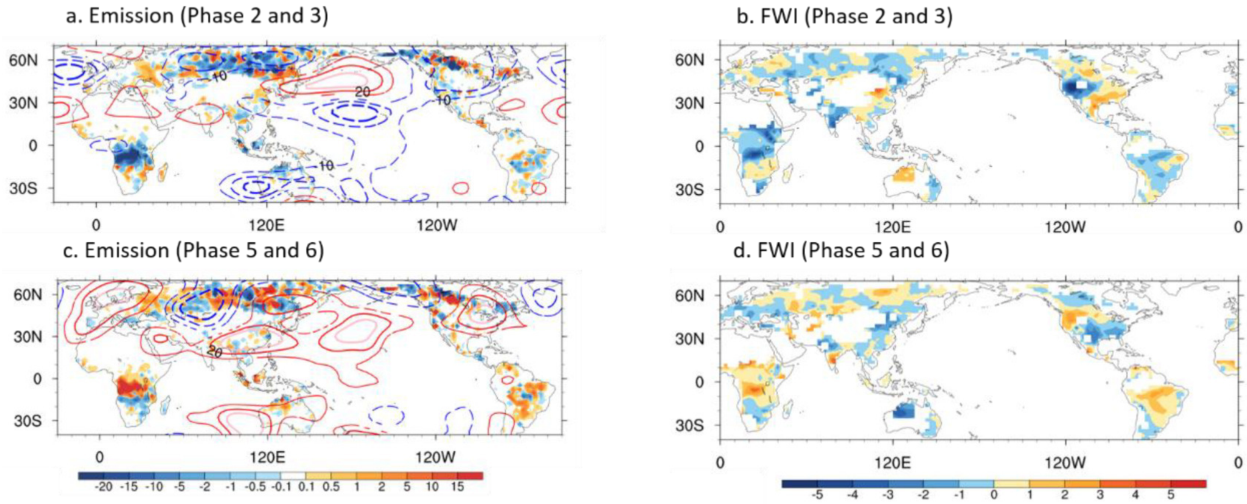

Fig. S4. Emissions and fire weather index (FWI) during active MJO. (a, b) Composite May–July (a) wildfire emission and (b) FWI anomalies during MJO phases 2 and 3. (c, d) As in (a, b) but during MJO phases 5 and 6. The years 2003–20 and 20–100-day bandpass-filtered data are used for the analysis.

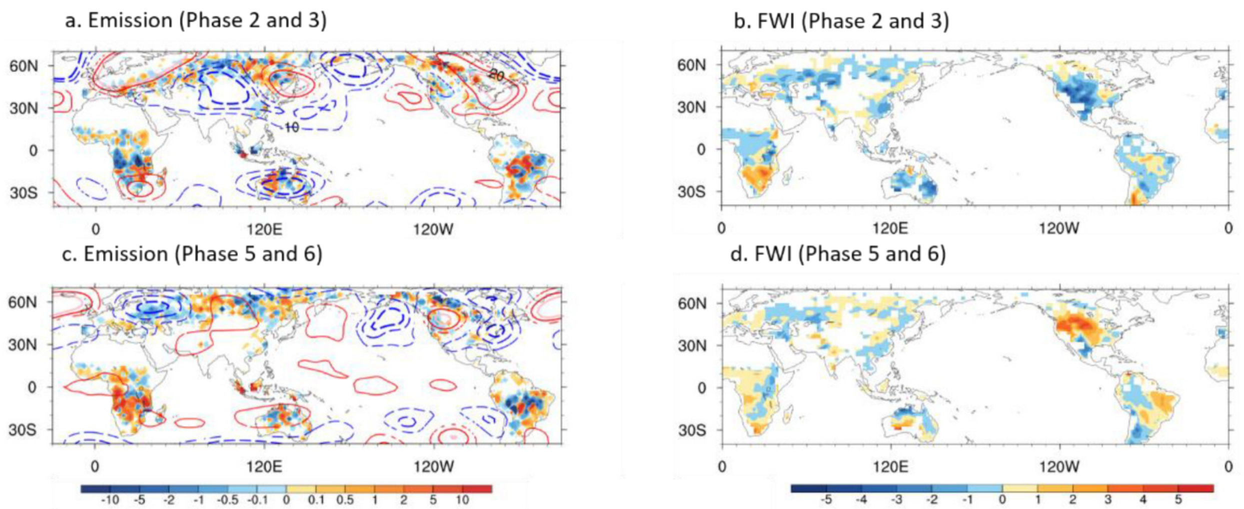

Fig. S5. Emissions and fire weather index (FWI) during active MJO. (a, b) Composite August–October (a) wildfire emission and (b) FWI anomalies during MJO phases 2 and 3. (c, d) As in (a, b) but during MJO phases 5 and 6. Eighteen years (2003–20) of 20–100-day bandpass-filtered data are used for the analysis.

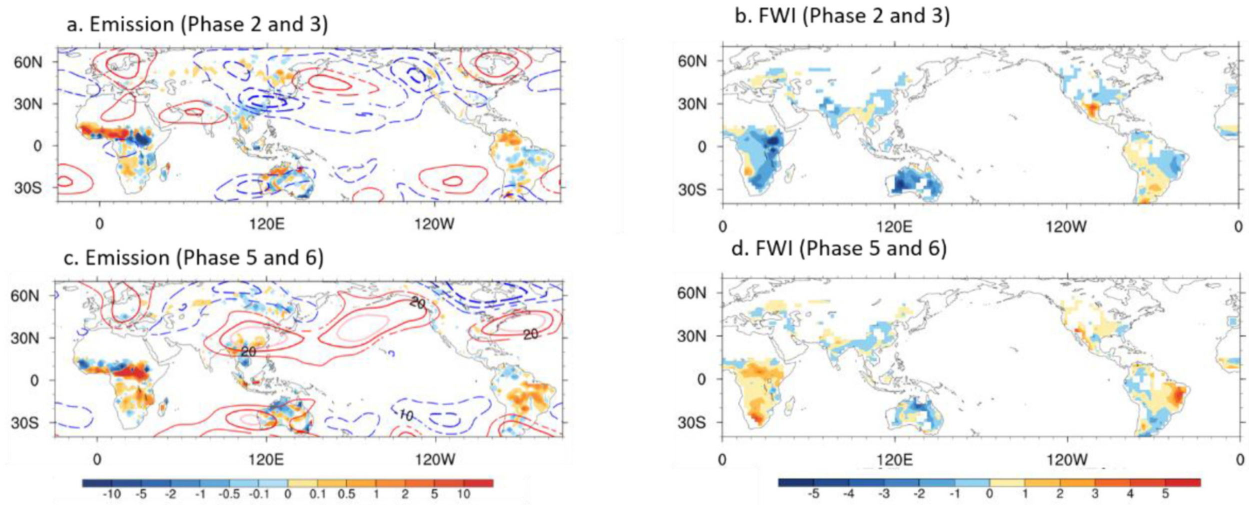

Fig. S6. Emissions and fire weather index (FWI) during active MJO. (a, b) Composite November–January (a) wildfire emission and (b) FWI anomalies during MJO phases 2 and 3. (c, d) As in (a, b) but during MJO phases 5 and 6. Eighteen years (2003–20) of 20–100-day bandpass-filtered data are used for the analysis.

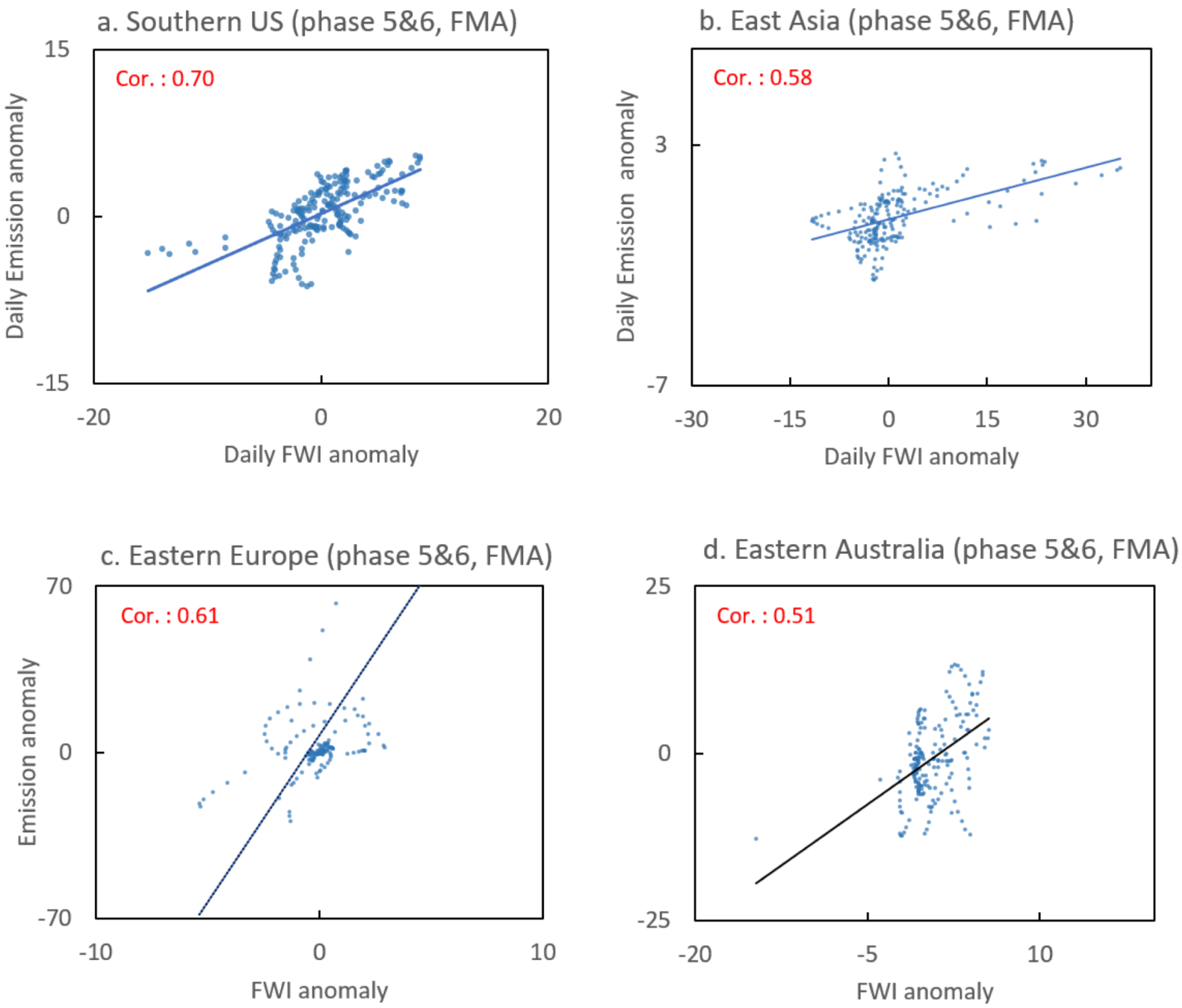

Fig. S7. Strong relationship between emission and FWI anomalies. (a–c) Scatter plots of February–April 20–70-day filtered daily wildfire emission and FWI anomalies in (a) the southern US, (b) East Asia, (c) eastern Europe, and (d) eastern Australia during MJO phases 5 and 6. Eighteen years (2003–20) of data are used. The red values are correlation coefficients.

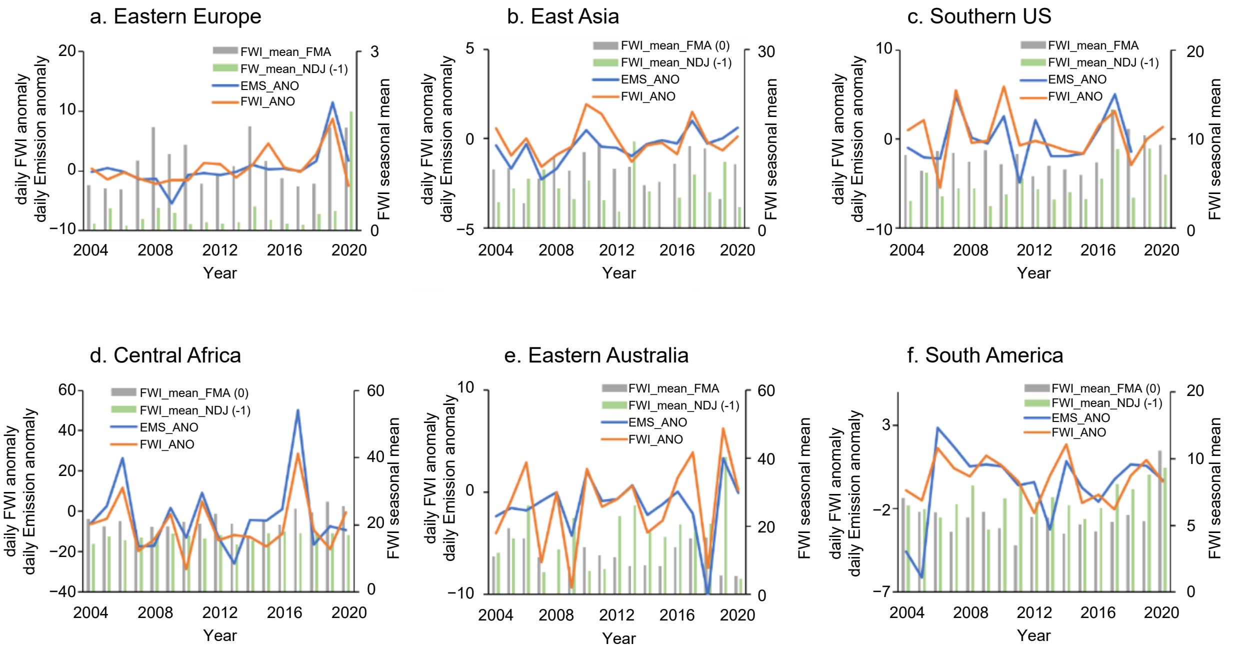

Fig. S8. Impact of background climate on MJO-related wildfire. Interannual variability of composite February–April wildfire emission and fire weather index (FWI) anomalies during MJO phases 2 and 3 in (a) eastern Europe, (b) East Asia, (c) the southern US, (d) central Africa, (e) eastern Australia, and (f) South America. The blue (orange) line represents emission (FWI) anomalies. The gray bars denote the February–April-mean FWI, and green bars the November–January-mean FWI, of the previous year. Data for the years 2003–20 are used.

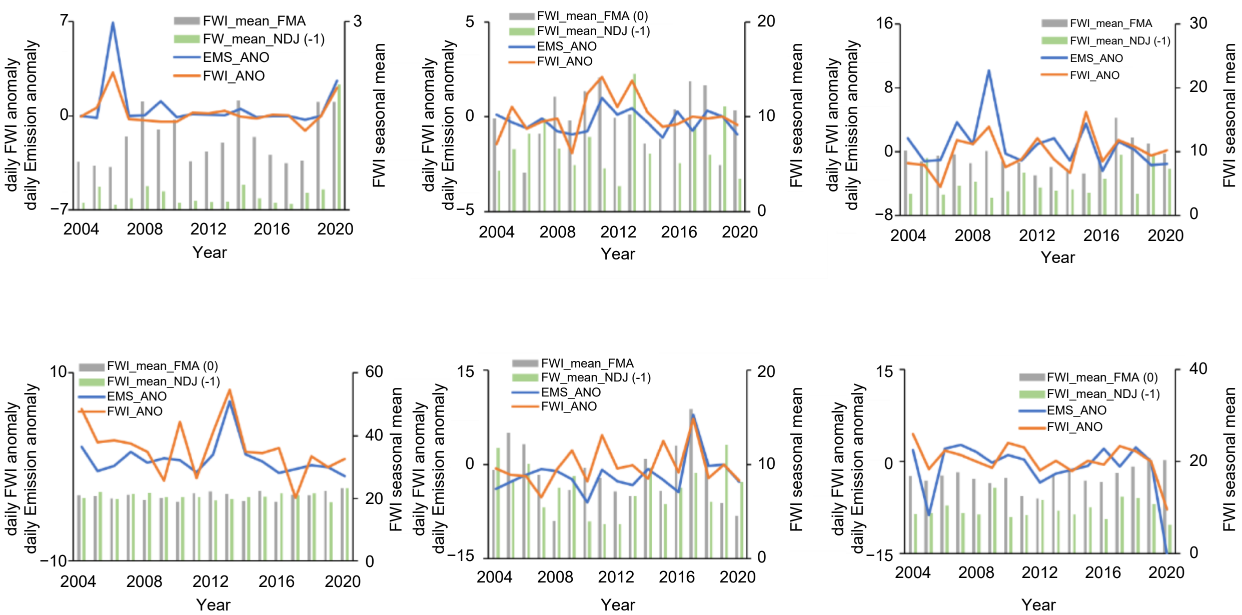

Fig. S9. Impact of background climate on MJO-related wildfire. Interannual variability of composite February–April wildfire emission and fire weather index (FWI) anomalies during MJO phases 5 and 6 in (a) eastern Europe, (b) East Asia, (c) the southern US, (d) central Africa, (e) eastern Australia, and (f) South America. The blue (orange) line represents emission (FWI) anomalies. The gray bars denote the February–April-mean FWI, and green bars the November–January-mean FWI, of the previous year. Data for the years 2003–20 are used.

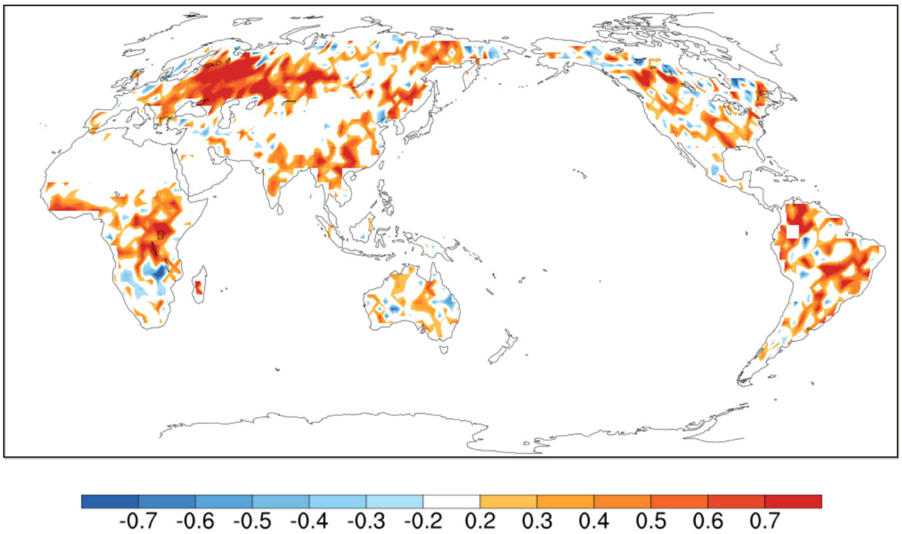

Fig. S10. Interannual variability of MJO-related wildfire. Horizontal map of correlation coefficients between February–April wildfire emission and fire weather index (FWI) anomalies during MJO phases 2 and 3. Annual composite data are used for analysis. Data for the years 2003–20 are used.